Solution Conformation of the (+)-*cis*-*anti*-[BP]dG Adduct opposite a Deletion Site in a DNA Duplex: Intercalation of the Covalently Attached Benzo[a]pyrene into the Helix with Base Displacement of the Modified Deoxyguanosine into the Minor Groove†

Monique Cosman,‡ Radovan Fiala,‡ Brian E. Hingerty,§ Shantu Amin,∥ Nicholas E. Geacintov,⊥ Suse Broyde,# and Dinshaw J. Patel*,‡

Cellular Biochemistry and Biophysics Program, Memorial Sloan-Kettering Cancer Center, New York, New York 10021, Health and Safety Research Division, Oak Ridge National Laboratory, Oak Ridge, Tennessee 37831, American Health Foundation, Valhalla, New York 10595, and Chemistry and Biology Departments, New York University, New York, New York 10003

Received April 27, 1994; Revised Manuscript Received July 28, 1994®

ABSTRACT: We have applied a combined NMR–molecular mechanics approach to determine the solution structure of the (+)-*cis*-*anti*-[BP]dG adduct positioned opposite a deletion site in the sequence d(C5-[BP]G6-C7)·d(G16-G17) at the DNA oligomer duplex level. Our structural studies establish that the benzo[a]pyrene ring intercalates into the helix opposite the deletion site while the modified deoxyguanosine is displaced into the minor groove with its plane parallel to the helix axis. The intercalation site is wedge-shaped with the benzo[a]pyrene ring stacked over intact flanking Watson–Crick dG·dC base pairs. The modified deoxyguanosine stacks over the minor groove face of the sugar ring of the 5′-flanking dC5 residue. The structure at the lesion site is consistent with the observed intermolecular NOEs which served as input restraints to guide the molecular mechanics calculations, and, in addition, the various stacking interactions explain the observed large ring current shifts associated with adduct formation. The solution structure of the (+)-*cis*-*anti*-[BP]dG adduct positioned opposite a deletion site reported in this study is similar to the corresponding structure of the same adduct positioned opposite dC reported previously [Cosman, M., de los Santos, C., Fiala, R., Hingerty, B. E., Luna, E., Harvey, R. G., Geacintov, N. E., Broyde, S., & Patel, D. J. (1993) *Biochemistry 32,* 4145–4155]. This is not surprising since the dC opposite the lesion site was looped out of the helix and it can be readily replaced by a deletion site through minor changes associated with buckling of the intercalation site. By contrast, the solution structures of the (+)-*trans*-*anti*-[BP]dG and (+)-*cis*-*anti*-[BP]dG adducts positioned opposite deletion sites in the same sequence context exhibit distinct surface topologies in the grooves of the DNA helix. Thus, even though the benzo[a]pyrene intercalates into the helix opposite the deletion site in both cases, the modified deoxyguanosine is displaced into the major groove for the (+)-*trans*-*anti*-[BP]dG adduct while it is displaced into the minor groove for the (+)-*cis*-*anti*-[BP]dG stereoisomer. The orientational differences reflect the chiral characteristics of the two [BP]-dG stereoisomeric adducts with the different alignments of the bulky DNA lesion opposite the deletion site likely to influence interactions with the cellular repair machinery.

Of the four biologically active stereoisomeric bay region diol epoxides derived from the metabolic activation of the environmental pollutant benzo[a]pyrene (BP), the (+)-*anti*-7,8-dihydroxy-9,10-epoxy-7,8,9,10-tetrahydro isomer [(+)-*anti*-BPDE] is the most tumorigenic and mutagenic in mammalian systems [reviewed in Conney (1982) and Harvey (1991)]. Although the mechanism of tumor induction is not yet well understood, it is believed that the critical initial step in the multistage process of (+)-*anti*-BPDE induced carcinogenesis involves genetic damage resulting from covalent modification of cellular DNA (Jeffrey et al., 1976; Koreeda et al., 1978; Yang et al., 1987; Stevens et al., 1985; Miller et al., 1985; Pruess-Schwartz & Baird, 1986). (+)-*anti*-BPDE can covalently bind to the exocyclic amino group of deoxyguanosine (N^2-dG) by either *trans* or *cis* addition at the C^{10} position (Cheng et al., 1989; Cosman, 1991). Although the predominant product of the reaction of (+)-*anti*-BPDE with DNA is the (+)-*trans*-anti-N^2-[BP]-dG adduct (Jeffrey et al., 1976), little is known about the relative tumorigenic potentials of the other stereospecifically defined adducts. Therefore, although the (+)-*cis*-*anti*-[BP]dG adduct is a relatively minor product, its contribution to the overall biological activity of (+)-*anti*-BPDE may be important.

Previously, we have used two-dimensional NMR and computational methods to obtain the solution structure of the (+)-*cis*-*anti*-[BP]dG·dC 11-mer duplex where the [BP]dG adduct was positioned opposite dC in the duplex (Cosman et al., 1993). The results established that the pyrenyl ring of the covalently attached carcinogen intercalated into the helix and stacked between intact flanking dG·dC base pairs. This resulted in disruption of the modified base pair with the modified deoxyguanosine base being displaced into the minor groove and parallel to the helical axis while the deoxycytidine

† This research was supported by NIH Grant CA-46533 to D.J.P., by NIH CA-20851 and DOE Grant DE-FG02-88ER60405 to N.E.G., by NIH Grant CA-28038, NIH Grant RR-06458 and DOE Grant DE-FG02-90ER60931 to S.B., and by DOE Contract DE-AC05-840R21400 with Martin-Marietta Energy Systems and DOE OHER Field Work Proposal ERKP931 to B.E.H.

* Author to whom correspondence should be addressed.
‡ Memorial Sloan-Kettering Cancer Center.
§ Oak Ridge National Laboratory.
∥ American Health Foundation.
⊥ Chemistry Department, New York University.
Biology Department, New York University.

® Abstract published in *Advance ACS Abstracts,* September 1, 1994.

0006-2960/94/0433-11518$04.50/0

was displaced into the major groove.

The novel structure obtained for the (+)-*cis*-*anti*-[BP]-dG·dC 11-mer duplex suggested the possibility that the displaced modified deoxyguanosine may not participate in base pairing and result in a deletion mutation during replication. The types of mutations induced by racemic BPDE have been studied in the *supF* tRNA gene of the pZ189 shuttle vector replicating in human cell lines (Yang et al., 1987; Maher et al., 1989), in the dihydrofolate reductase gene in Chinese hamster ovary cells (Carothers & Grunberger, 1990), in the endogeneous *aprt* gene in Chinese hamster ovary cells (Mazur & Glickman, 1988), in *Escherichia coli* plasmids (Mizusawa et al., 1981), in the *hprt* gene in diploid human fibroblasts (Yang et al., 1991), in mutants of cultured human lymphoblastoid cells (Keohavong & Thilly, 1992), and in the *lacI* gene of excision repair-deficient (Uvr⁻) *E. coli* (Bernelot-Moens et al., 1990). Several more recent studies have focused on the mutagenic specificity of the (+)-*anti*-BPDE in the *supF* gene of a plasmid (pUB3) transfected in *E. coli* cells (Rodriguez & Loechler, 1993) and in the *hprt* gene of Chinese hamster V-79 cells (Wei et al., 1991, 1993). Base substitution mutations are dominant, but in most cases a smaller fraction of the mutations consist of −1 base (or larger) deletions leading to frame-shift mutations. The general mechanisms of deletion mutations (Streisinger et al., 1966; Kunkel, 1990), and especially the role of bulky adducts in these processes (Kunkel, 1990; Schaaper et al., 1990; Lambert et al., 1992; Shibutani & Grollman, 1993) have been discussed. In these models, the bulky carcinogen residues cause the polymerases to stall, resulting in the formation of transient misaligned template–primer intermediates in which one or more bases on the primer strand bulge out while the remaining base pairs retain hydrogen-bonded alignments. If extension of the primer continues when the primer–template complex is misaligned, a deletion mutation ensues.

Recently, the mutagenic characteristics of stereochemically distinct and site-specific *anti*-[BP]dG lesions situated in defined DNA sequences in an *E. coli* plasmid have been evaluated in site-directed mutagenesis experiments (Mackay et al., 1992) and in DNA polymerase-catalyzed primer extension experiments *in vitro* (Hruszkewycz et al., 1992; Shibutani et al., 1993). It was shown that the (+)-*cis*-*anti*-[BP]dG lesion is a more effective block to replication than the (+)-*trans*-*anti*-[BP]dG adduct (Hruszkewycz et al., 1992) and that a sizeable fraction of mutations in the extended primers were −1 and −2 base deletions or frame-shift mutations (Shibutani et al., 1993).

In order to gain a better understanding of the structural basis for frame-shift mutations, we have used a combined NMR–molecular mechanics study to determine the solution conformation of the (+)-*cis*-*anti*-[BP]dG adduct [see **2** in Cosman et al. (1994)] positioned opposite a deletion site within the d(C-[BP]G-C)·d(G-G) sequence context [see **3** in Cosman et al. (1994)] of the (+)-*cis*-*anti*-[BP]dG·del 11-mer duplex.

MATERIALS AND METHODS

Preparation of the (+)-cis-anti-[BP]dG·del 11-mer Duplex. We have previously described the preparation and purification of the (+)-*cis*-*anti*-[BP]dG adduct embedded in the d(C-C-A-T-C-[BP]G-C-T-A-C-C) sequence context (Cosman et al., 1993). This modified 11-mer strand was annealed with the complementary d(G-G-T-A-G-G-A-T-G-G) 10-mer strand at 70 °C, and the stoichimetry followed by monitoring single proton resonaces in both strands.

NMR Experiments. NMR studies were undertaken on the (+)-*cis*-*anti*-[BP]dG·del 11-mer duplex (~5 mg) in aqueous buffer (0.6 mL in 0.1 M NaCl, 10 mM phosphate, 0.1 mM EDTA, pH 7.0). A set of NOESY experiments was recorded in H_2O and D_2O solution along with COSY, HOHAHA, and heteronuclear ^1H–^{31}P correlation experiments in D_2O. Details are provided in the preceding paper in this issue (Cosman et al., 1994).

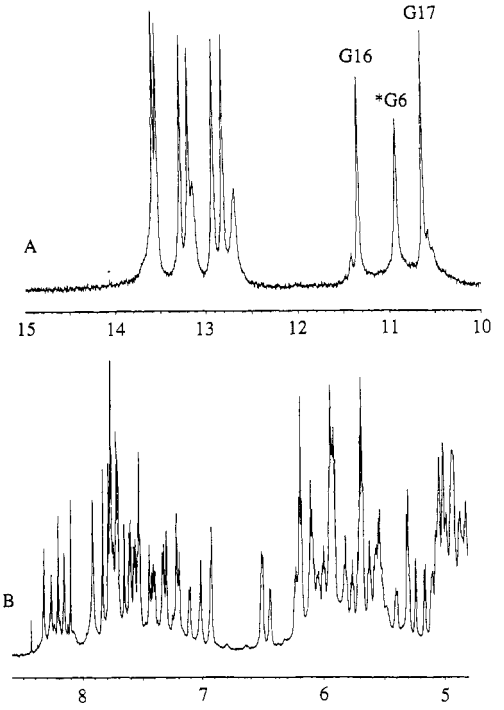

FIGURE 1: (A) Imino proton spectrum (10.0–15.0 ppm) in H_2O buffer at 1 °C and (B) nonexchangeable proton spectrum (4.8–8.6 ppm) in D_2O buffer at 25 °C of the (+)-*cis*-*anti*-[BP]dG·del 11-mer duplex. The buffer was 0.1 M NaCl and 10 mM phosphate, aqueous solution, pH 7.0. The imino protons of [BP]dG6, dG16 and dG17 are assigned over spectrum A.

Molecular Mechanics Computations. Details of the application of the DUPLEX molecular mechanics program that undertakes potential energy minimization computations in the reduced variable domain of torsion angle space are described in the preceding paper (Cosman et al., 1994).

RESULTS

We have measured the thermal transition midpoints at optical concentrations (~10 μM in strands) for the control dG·del 11-mer duplex (t_m = 24 °C) and the (+)-*cis*-*anti*-[BP]dG·del 11-mer duplex (t_m = 49 °C). This remarkable stabilization on adduct formation permits us to undertake NMR studies (at millimolar concentrations) on the (+)-*cis*-*anti*-[BP]dG·del 11-mer duplex at ambient temperature.

Exchangeable Proton Spectra. The exchangeable imino proton spectrum (10.0–14.0 ppm) of the (+)-*cis*-*anti*-[BP]-dG·del 11-mer duplex in H_2O buffer, pH 7.0, at 1 °C is plotted in Figure 1A. A set of resolved imino protons are detected between 12.5 and 13.8 ppm along with the three imino protons which exhibit unusual upfield shifts at 11.37, ~11.0, and 10.66 ppm. The imino protons have been assigned by recording NOE connectivities in expanded NOESY (150-ms mixing time) contour plots of the adduct duplex in H_2O buffer at 1 °C (Figure 2). We can detect NOEs between adjacent imino protons from dG13 to dG16 and from dG17 to dG20 on either side of the [BP]dG6 lesion site (Figure 2A). However, we do not detect NOEs from the imino protons of either dG16 or dG17 to the imino protons of [BP]dG6 (Figure 2A) nor do we detect an NOE between the imino protons of dG16 and

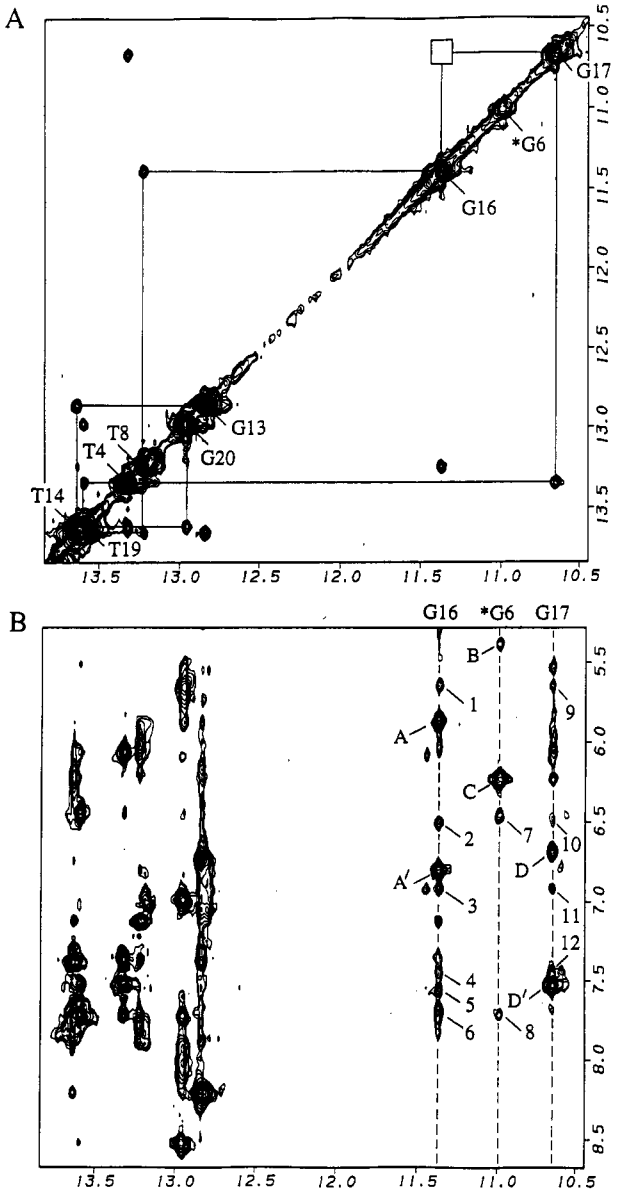

FIGURE 2: Expanded NOESY (150-ms mixing time) contour plots of the (+)-*cis*-*anti*-[BP]dG·del 11-mer duplex in H_2O buffer, pH 7.0, at 1 °C. (A) NOE connectivities in the symmetrical 10.5–14.0 ppm region. The imino proton assignments are labeled along the diagonal. The lines trace the NOE connectivities between imino protons on adjacent base pairs starting at dG20 toward one end of the helix and proceeding to dG13 toward the other end of the helix. This connectivity tracing is broken between the imino protons of dG16 and dG17. (B) NOE connectivities between the imino protons (10.5–14.0 ppm) and the base and amino protons (5.5–8.5 ppm). The imino protons of [BP]dG6, dG16, and dG17 centered about the lesion site are labeled in the figure. The intramolecular cross peaks A–D between nucleic acid protons are assigned as follows: (A,A') G16-(NH1)-C7(NH_2-4b,e); (B) [BP]G6(NH1)-C5(H1'); (C) [BP]G6-(NH1)-[BP]G6(NH_2-2); (D,D') G17(NH1)-C5(NH_2-4b,e). The intermolecular cross peaks 1–12 are assigned as follows: (1) G16-(NH1)-BP(H4); (2) G16(NH1)-BP(H5); (3) G16(NH1)-BP(H3); (4) G16(NH1)-BP(H2/H12); (5) G16(NH1)-BP(H1); (6) G16-(NH1)-BP(H6); (7) [BP]G6(NH1)-BP(H10); (8) [BP]G6(NH1)-BP(H11); (9) G17(NH1)-BP(H4); (10) G17(NH1)-BP(H5/H10); (11) G17(NH1)-BP(H3); (12) G17(NH1)-BP(H2/H12).

dG17 (boxed region, Figure 2A). This analysis establishes that the narrow imino protons of dG16 (11.37 ppm) and dG17 (10.66 ppm) have been shifted dramatically to high field in the adduct duplex.

We also detect NOEs between the deoxyguanosine imino and deoxycytidine amino protons for the dC5·dG17 (peaks D and D', Figure 2B) and the dC7·dG16 (peaks A and A', Figure 2B) base pairs establishing Watson–Crick dG·dC alignment adjacent to the deletion site. The deoxycytidine amino protons of dC7 (5.86, 6.70 ppm) to a greater extent, and dC5 (6.70, 7.53 ppm) to a lesser extent, are also shifted to high field in the adduct duplex. These large upfield shifts for the deoxyguanosine imino and deoxycytidine amino protons of the dC5·dG17 and dC7·dG16 base pairs are consistent with intercalation of the pyrenyl ring of [BP]dG6 into the helix between these base pairs.

Table 1: Proton Chemical Shifts of the d(C5-[BP]G6–C7)·d(G16–G17) Segment of the (+)-*cis*-*anti*-[BP]dG·del 11-mer Duplex in Aqueous Buffer

	exchangeable proton chemical shifts (ppm), 1 °C		
	G(NH1)	G(NH_2-2)	C(NH_2-4)
dC5·dG17	10.66		6.70,[a] 7.53[b]
dC7·dG16	11.37		5.86,[a] 6.81[b]
[BP]dG6	11.00	6.24	

	nonexchangeable proton chemical shifts (ppm), 25 °C					
	H8/H6	H2/H5	H1′	H2′, H2″	H3′	H4′
dC5	7.11	5.56	5.41	2.50, 1.20	4.93	3.64
[BP]dG6	8.11		6.52	2.70, 3.50	5.12	4.75
dC7	7.54	5.17	4.33	1.81, 2.07	4.45	4.22
dG16	7.71		5.96	2.53, 2.49	5.06	4.49
dG17	7.92		5.53	2.52, 2.68	5.06	4.51

[a] Exposed amino proton. [b] Hydrogen-bonded amino proton.

The imino proton of [BP]dG6 is also shifted upfield to ~11.0 ppm, but this shift reflects displacement of the modified deoxyguanosine out of the helix following intercalation of the pyrenyl ring. The upfield chemical shift and broadening of its line width at elevated temperatures reflects exposure of the imino proton of [BP]dG6 to solvent following base displacement of the deoxyguanosine out of the helix. The corresponding amino proton of [BP]dG6 resonates at 6.24 ppm in the adduct duplex.

The exchangeable imino and amino proton chemical shifts for the central d(C5-[BP]G6-C7)·d(G16-G17) segment of the (+)-*cis*-*anti*-[BP]dG·del 11-mer duplex at 1 °C are listed in Table 1. The exchangeable proton chemical shift assignments for the entire adduct duplex are listed in Table S1 (Supplementary Material).

Nonexchangeable Nucleic Acid Protons. The nonexchangeable base and sugar H1′ proton spectrum (5.0–8.5 ppm) of the (+)-*cis*-*anti*-[BP]dG•del 11-mer duplex in D_2O buffer, pH 7.0, at 25 °C is plotted in Figure 1B. The spectrum exhibits extremely well resolved resonances which has permitted assignments of both the benzo[a]pyrene and DNA protons in the adduct duplex. An expanded NOESY contour plot (300-ms mixing time) correlating the base protons (6.8–8.4 ppm) with the sugar H1′ and H3′ protons (4.2–4.7 ppm; 5.0–6.6 ppm) for the adduct duplex at 25 °C is plotted in Figure 3. We have traced the NOE connectivities between the base and its own and 5′-flanking sugar H1′ protons for the d(T4-C5-[BP]G6-C7-T8) segment of the modified strand (solid line, Figure 3) and the d(A15-G16-G17-A18) segment on the deletion strand (dashed line, Figure 3).

The NOEs between adjacent residues are absent for the dC5-[BP]dG6 step and very weak for the dT4-dC5 and [BP]-dG6-dC7 steps on the modified strand. Further, no NOE is detected between the H8 proton of [BP]dG6 and the H5 proton of dC7 at the purine (3′–5′) pyrimidine step indicative of a structural distortion centered about the lesion site.

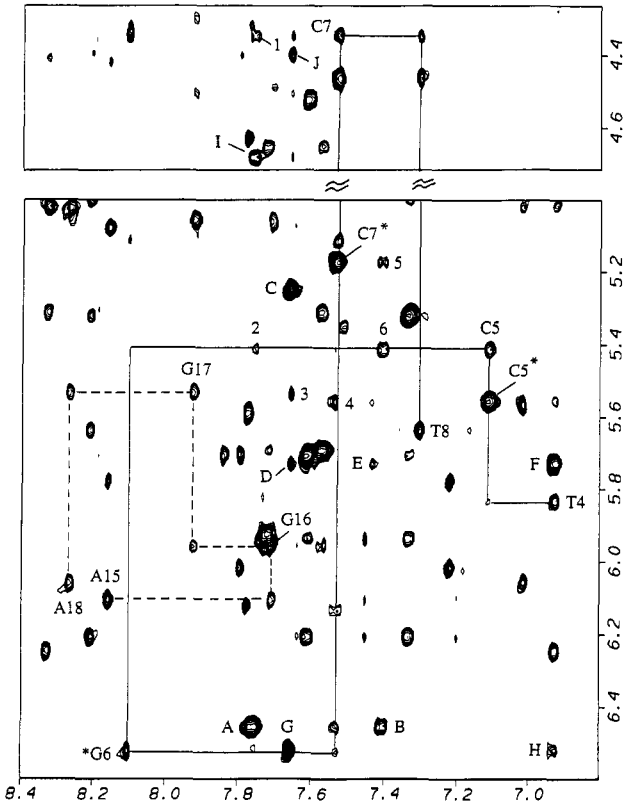

FIGURE 3: Expanded NOESY (300-ms mixing time) contour plot of the (+)-*cis*-*anti*-[BP]dG·del 11-mer duplex in D_2O buffer at 25 °C establishing distance connectivities between the base (purine H8 and pyrimidine H6) protons (6.8–8.4 ppm) and the sugar H1′ and H3′ and deoxycytidine H5 protons (4.3–4.7 ppm; 5.0–6.6 ppm). The NOE connectivities between the base and their own and 5′-flanking sugar H1′ protons from dT4 to dT8 on the modified strand are shown by solid lines and from dA15 to dA18 on the unmodified strand are shown by dashed lines. The assignments label the base to their own sugar H1′ NOEs, while the deoxycytidine H6–H5 NOEs are designated by asterisks. Note the unusual upfield shift of the H1′ proton of dC7 and to a lesser extent the upfield shifts of the H6 and H5 protons of dC7 labeled by cross peak C7* and the downfield shift of the H1′ proton of [BP]dG6. Note that the cross peaks linking the dC5-[BP]dG6 step are missing while the cross peaks linking the dT4-dC5 and [BP]dG6-dC7 steps are very weak. The intramolecular cross peaks A–J between benzo[a]pyrene protons are assigned as follows: (A) BP(H10)-BP(H11); (B) BP(H10)-BP(H12); (C) BP-(H6)-BP(H7); (D) BP(H4)-BP(H6); (E) BP(H2)-BP(H4); (F) BP-(H3)-BP(H4); (G) BP(H5)-BP(H6); (H) BP(H3)-BP(H5); (I) BP(H9)-BP(H11); (J) BP(H6)-BP(H8). The intermolecular cross peaks 1–6 are assigned as follows: (1) C7(H1′)-BP(H11); (2) C5-(H1′)-BP(H11); (3) C17(H1′)-BP(H6); (4) C5(H5)-BP(H1); (5) C5(H5)-BP(H12); (6) C5(H1′)-BP(H12). The chemical shift values for the benzylic protons are BP(H7), 5.24 ppm; BP(H8), 4.39 ppm; BP(H9), 4.68 ppm; BP(H10), 6.45 ppm. The chemical shift values for the pyrenyl protons are BP(H11), 7.76 ppm; BP(H12), 7.41 ppm; BP(H1), 7.54 ppm; BP(H2), 7.43 ppm; BP(H3), 6.94 ppm; BP(H4), 5.72 ppm; BP(H5), 6.51 ppm; BP(H6), 7.66 ppm.

The orientation of the dexoyguanosyl ring of [BP]dG6 within the d(C5-[BP]G6-C7) segment is defined by NOEs detected between the base protons of [BP]dG6 and the minor groove sugar protons of dC5 in the adduct duplex. These include NOEs between the H8 proton of [BP]dG6 and the H4′ proton of dC5 (peak A, Figure S1, Supplementary Material) and between the imino proton of [BP]dG6 and the H1′ proton of dC5 (peak B, Figure 2B). These results establish that the deoxyguanosine of [BP]dG6 is displaced out of the helix into the minor groove and is oriented toward the 5′-end of the modified strand.

The nonexchangeable base and sugar proton chemical shifts have been assigned and cross-checked following analysis of

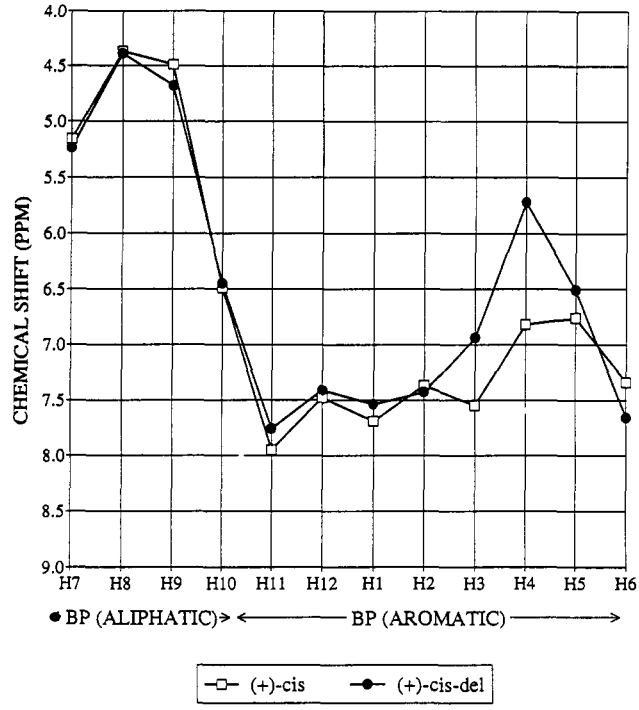

FIGURE 4: Plot comparing the benzo[a]pyrene ring proton chemical shifts in the (+)-*cis*-*anti*-[BP]dG·dC 11-mer duplex (□) and the (+)-*cis*-*anti*-[BP]dG·del 11-mer duplex (●). The benzylic protons (H7, H8, H9, H10) are on the left and the pyrenyl protons (H11, H12, H1, H2, H3, H4, H5, H6) are on the right of this plot.

the complete NOESY and COSY data sets, and the values for the d(C5-[BP]G6-C7)·d(G16-G17) segment of the (+)-*cis*-*anti*-[BP]dG·del 11-mer duplex at 25 °C are listed in Table 1. The nonexchangeable proton chemical shift assignments for the entire adduct duplex are listed in Table S2 (Supplementary Material). The corresponding exchangeable and nonexchangeable proton complexation shifts on proceeding from the control dG·del 11-mer duplex to the adduct duplex are listed in Table S3.

Several proton resonances of the d(C5-[BP]G6-C7) segment in the adduct duplex exhibit unusual chemical shifts reflecting ring current contributions from nearby aromatic ring systems. The H2″ (1.20 ppm), H4′ (3.64 ppm), and H5 (5.57 ppm) protons of dC5 and the H1′ (4.33 ppm) proton of dC7 are shifted to high field while the H1′ (8.11 ppm) and H2″ (3.50 ppm) protons of [BP]dG6 are shifted to low field in the adduct duplex (Table 1).

The majority of the sugar rings in the adduct duplex exhibit puckers in the C2′-*endo* range based on the magnitude of the base proton to its own and 5′-flanking sugar proton NOEs and on the coupling constant patterns between the sugar H1′ and sugar H2′, 2″ protons for individual sugars. The only exception is the dC5 sugar which exhibits a C3′-*endo* pucker based on a strong base H6 to its own sugar H3′ NOE at short (50-ms) mixing time, as well as on a weak H1′–H2′ coupling (2.5 Hz) and a strong H3′–H4′ coupling (~8 Hz) between vicinal proton pairs.

Nonexchangeable Benzo[a]pyrene Protons. The benzylic and pyrenyl protons of [BP]dG6 in the (+)-*cis*-*anti*-[BP]-dG·del 11-mer duplex have been assigned following analysis of the through-space and through-bond connectivities involving these protons. The chemical shifts are listed in the caption to Figure 3 and graphically presented in Figure 4. The majority of the benzylic protons are shifted to high field of 8.0 ppm with the largest upfield shifts detected at the H3

Table 2: Comparison of Input Interproton Distance Bounds with Those Observed for the Solution Structure of the (+)-*cis*-*anti*-[BP]dG·del 11-mer Duplex

	interproton distances (Å)	
	experimental bounds	observed
exchangeable protons		
[BP]G6(NH1)–BP(H10)	3.0–4.5	4.29
[BP]G6(NH2)–BP(H10)	3.0–4.5	2.84
G16(NH1)–BP(H3)	3.0–4.5	5.80
G16(NH1)–BP(H5)	2.5–4.0	3.65
G17(NH1)–BP(H4)	3.0–4.5	4.72
nonexchangeable protons		
C5(H1′)–BP(H12)	4.0–5.5	4.33
C5(H2′)–BP(H12)	3.5–5.0[a]	2.37
C5(H2″)–BP(H12)	3.5–5.0	3.78
C5(H3′)–BP(H12)	4.5–6.0	4.24
C5(H5)–BP(H1)	3.5–5.0	3.54
C5(H6)–BP(H12)	3.5–5.0	4.02
[BP]G6(H1′)–BP(H10)	3.5–5.0	4.91
[BP]G6(H2′)–BP(H12)	4.0–5.0	5.06
[BP]G6(H2″)–BP(H11)	4.0–6.0	4.43
C7(H1′)–BP(H10)	3.5–5.5	4.34
C7(H5)–BP(H12)	4.0–5.5	3.72
G17(H1′)–BP(H6)	3.5–5.0	3.29

[a] Partially overlapped cross peak.

(6.94 ppm), H4 (5.72 ppm), and H5 (6.51 ppm) protons in the adduct duplex.

Previous NMR studies of various stereoisomeric [BP]dG adducts at the DNA duplex level have been hampered by the near degeneracy of the proton chemical shifts of the BP(H8) and BP(H9) benzylic ring protons. By contrast, the BP(H8) proton (4.39 ppm) is sufficiently well resolved from the BP(H9) proton (4.68 ppm) so that both the NOE and the coupling constant pattern can be detected between them in the (+)-*cis*-*anti*-[BP]dG·del 11-mer duplex. The experimental coupling cross peak patterns for the benzylic protons and their simulated counterparts show good agreement for proton–proton coupling constant values of ^3J(H7,H8) = 3.0 ± 0.5 Hz, ^3J(H8,H9) = 3.5 ± 0.5 Hz, and ^3J(H9,H10) = 5.5 ± 0.5 Hz. These coupling constants restrict the pucker of the benzylic ring to a specific distorted half-chair conformation where the BP(H7), BP(H8), and BP(H10) adopt pseudoequatorial orientations while BP(H9) adopts a pseudoaxial orientation.

Intermolecular NOEs. We have identified and assigned a set of intermolecular NOEs between the exchangeable and nonexchangeable nucleic acid protons and nonexchangeable BP protons in the (+)-*cis*-*anti*-[BP]dG·del 11-mer duplex. Several of these intermolecular NOEs are labeled by numbers in the expanded NOESY contour plot of the exchangeable protons in H_2O solution (Figure 2B) and in the expanded NOESY contour plot of nonexchangeable protons in D_2O solution (Figure 3) with the cross peak assignments listed in the figure captions. Seventeen of these intermolecular distance restraints defined by lower and upper bounds for the central d(C5-[BP]G6-C7)·d(G16-G17) segment that were used to guide the computations are listed in Table 2. Another 10 weak intermolecular NOEs that were observed but not used in the computations are listed in Table S4 (Supplementary Material). A few more potential intermolecular constraints were not considered because of degeneracies in chemical shifts or severe cross peak overlaps.

The distribution of the observed intermolecular NOEs readily identifies the alignment of the intercalated pyrenyl ring relative to the d(C5-[BP]G6-C7) modified and d(G16-G17) deletion containing strands of the adduct duplex. We note that the long edge of the pyrenyl ring containing the H3, H4, H5, and H6 protons of BP exhibit NOEs primarily to the imino and sugar H1′ protons on the d(G16-G17) deletion containing strand (Tables 2 and S4). The other long edge of the pyrenyl ring containing the H10, H11, H12, and H1 protons exhibits NOEs to the base and sugar protons of the d(C5-[BP]G6-C7) modification containing strand (Tables 2 and S4). The benzylic ring is positioned in the minor groove based on the observed NOE between the benzylic BP(H10) and the minor groove C7(H1′) protons while the farthest pyrenyl ring is positioned in the major groove based on the observed NOE between the pyrenyl BP(H1) and major groove C5(H5) protons (Table 2). These intermolecular NOEs establish the orthogonal alignment of the long axis of the pyrenyl ring and the long axis of the flanking base pairs at the intercalation site in the adduct duplex.

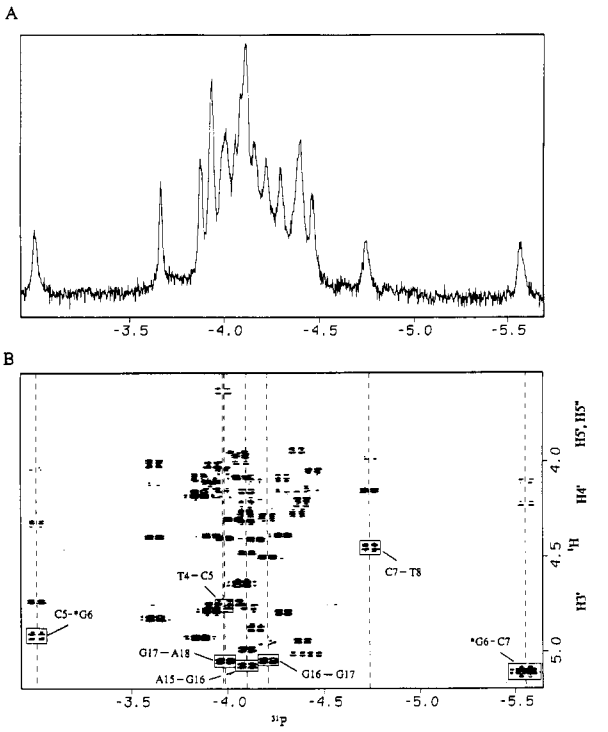

FIGURE 5: (A) Proton-decoupled phosphorus spectrum (–2.5 to –5.5 ppm upfield from standard trimethylphosphate) of the (–)-*trans*-*anti*-[BP]dG·del 11-mer duplex in D_2O buffer at 25 °C. (B) Expanded contour plot of the proton-detected phosphorus–proton heteronuclear correlation experiment on the (+)-*cis*-*anti*-[BP]dG·del 11-mer duplex in D_2O buffer at 25 °C. The phosphorus assignments for steps centered about the lesion site are listed. The correlation cross peaks between the phosphorus and its 5′-linked sugar H3′ protons are boxed.

Phosphorus Spectra. Two phosphorus resonances are shifted to low field and two others are shifted to high field of the central cluster of phosphorus resonances in the spectrum of the (+)-*cis*-*anti*-[BP]dG·del 11-mer duplex in D_2O at 25 °C (Figure 5A). The lowest and highest field phosphorus resonances are separated by 2.56 ppm, which is unusually large relative to an 0.5 ppm dispersion for unperturbed phosphorus resonances. We have assigned the phosphorus resonances in the adduct duplex spectrum following analysis of the proton–phosphorus correlation contour plot recorded at 25 °C (Figure 5B). The most downfield-shifted phosphorus is assigned to the d(C5-[BP]G6) step, while the most upfield-shifted phosphorus is assigned to the d([BP]G6-C7) step on the modified strand of adduct duplex. The phosphorus chemical shift differences between the control dG·del 11-mer duplex and the adduct duplex are plotted in Figure S2 (Supplementary Material). We observed large upfield shifts at the [BP]dG-C7 (~1.7 ppm) and the dC7-dT8 (~0.6 ppm)

steps on the modified strand and a large downfield shift at the dC5-[BP]dG6 step (~1.2 ppm) on the unmodified strand on proceeding from the control duplex to the adduct duplex (Figure S2).

Molecular Mechanics Computations. The proton and phosphorus chemical shift values, as well as the magnitude of the through-space intramolecular and intermolecular NOE patterns between proton pairs, exhibit striking similarities for the experimental data on the (+)-*cis*-*anti*-[BP]dG adduct positioned opposite dC (Cosman et al., 1993) and opposite a deletion site (this study). This implies common structural features for the (+)-*cis*-*anti*-[BP]dG adduct independent of whether it is positioned opposite dC or a deletion site at the DNA duplex level.

We therefore adopted the previously reported solution structure of the central d(C-[BP]G-C)·d(G-C-G) segment of the (+)-*cis*-*anti*-[BP]dG·dC 11-mer duplex (Cosman et al., 1993) except for deletion of the dC positioned opposite the [BP]dG lesion site as the starting model for the molecular mechanics calculations. The benzylic ring was fixed in the distorted half-chair conformation with BP(H7), BP(H8), and BP(H10) in pseudoequatorial orientations while BP(H9) was in a pseudoaxial orientation as defined by the coupling constant information. The DUPLEX hydrogen bond penalty function (Hingerty et al., 1989) for Watson–Crick pairing was utilized at all base pairs except for the unpaired [BP]dG6 residue, and the computations were guided by the NMR-based distance restraints defined by lower and upper bounds which are listed in Table 2.

The starting structure readily converged to its energy-minimized counterpart which satisfied the majority of the experimental distance restraints. The energy of this converged structure was −199 kcal/mol, and goodness-of-fit indices for eqs 1 and 2 of Cosman et al. (1994) were 3.0 and 12.1, respectively, with W = 15 kcal/mol·A^2. The F_N and F_{NN} values for the present structure of the (+)-*cis*-*anti*-[BP]dG·del 11-mer duplex are larger than those reported for the structure of the (+)-trans-anti-[BP]dG•del 11-mer duplex in the preceding paper. It should be noted, however, that one cannot assess relative goodness-of-fit for different molecules if these have different values of n, the number of target distances. Consequently, the converged structure was embedded in an energy-minimized B-form sequence corresponding to the adduct duplex and reminimized with all experimental restraints. Subsequently, the hydrogen bond penalty function and distance restraints were released with energy minimization in one step, yielding a final unrestrained structure for the (+)-*cis*-*anti*-[BP]dG·del 11-mer duplex.

Solution Structure. A view normal to the helix axis and looking into the minor groove for the central d(T4-C5-[BP]-G6-C7-T8)·d(A15-G16-G17-A18) segment of the lowest energy NMR energy-minimized structure of the (+)-*cis*-*anti*-[BP]dG·del 11-mer is shown in Figure 6A. Two views of the structure of the entire adduct duplex are shown in Figure S3 (Supplementary Material). The benzo[a]pyrene moiety which is covalently linked to the minor groove N^2 of dG6 intercalates between intact Watson–Crick dC5·dG17 and dC7·dG16 base pairs and in the process displaces the deoxyguanosine ring of [BP]dG6 into the minor groove (Figure 6A). The minor groove face of the sugar ring of dC5 is positioned over the deoxyguanosine base plane of [BP]dG6 which is directed toward the 5′-end of the modified strand and aligned approximately parallel to the helix axis. The intercalation site is wedge-shaped resulting in a shorter separation between base planes of dG16 and dG17 on the deletion containing

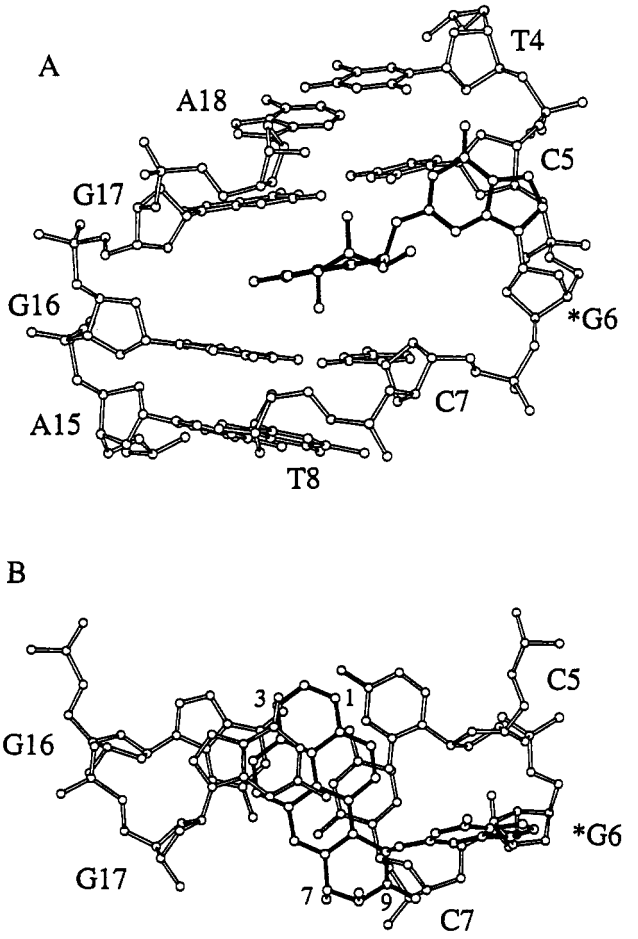

FIGURE 6: (A) View looking into the minor groove and normal to the helix axis for the d(T4-C5-[BP]G6-C7-T8)·d(A15-G16-G17-A18) segment in the solution structure of the (+)-*cis*-*anti*-[BP]dG•del 11-mer duplex. The BP ring system is shown in darkened bonds and is intercalated between the dC5·dG17 and dC7·dG16 base pairs which form a wedge-shaped intercalation site. The modified dG6 base is displaced into the minor groove and is directed toward the 5′-neighbor dC5 in the sequence. (B) View looking down the helix axis for the d(C5-[BP]G6-C7)·d(G16-G17) segment in the solution structure of the (+)-*cis*-*anti*-[BP]dG·del 11-mer duplex. Note that the benzylic ring is positioned in the minor groove while the pyrenyl ring stacks over the Watson–Crick hydrogen bonding regions of the flanking dC5·dG17 and dC7·dG16 base pairs. The minor groove edge of the dC5 sugar ring is positioned over the plane of the displaced modified dG6 residue.

strand relative to base planes of dC5 and dC7 on the modified strand (Figure 6A).

The long axis of the intercalated benzo[a]pyrenyl ring is approximately normal to the long axis of the flanking dC5·dG17 and dC7·dG16 base pairs with its benzylic ring positioned in the minor groove and the farthest aromatic ring on the pyrene extending into the major groove (Figure 6B). This intercalation orientation positions the pyrene ring directly over the Watson–Crick pairing edge of both flanking dG·dC base pairs (Figure 6B).

The benzylic ring of BP retains a distorted half-chair conformation with the BP(H7), BP(H8), and BP(H10) in pseudoequatorial orientations while BP(H9) adopts a pseudo-axial orientation. The carcinogen–base linkage site for the [BP]dG6 residue is defined by the angles α'[dG6(N^1)-dG6-(C^2)-dG6(N^2)-BP(C^{10})] = 169° and β'[dG6(C^2)-dG6(N^2)-BP(C^{10})-BP(C^9)] = 91° in the NMR energy-minimized structure of the (+)-*cis*-*anti*-[BP]dG·del 11-mer duplex.

The glycosidic torsion angles, sugar puckers, and backbone torsion angles for the d(T4-C5-[BP]G6-C7-T8)·d(A15-G16-

G17-A18) segment of the (+)-*cis-anti*-[BP]dG·del 11-mer duplex are listed in Table S5 (Supplementary Material). The glycosidic χ angle for [BP]dG6 is in the *anti* range but adopts an unusually low value of 168° in contrast to the usual values of about 230°–260° for B-DNA. The pseudorotation **P** value of 41° for dC5 defines this sugar pucker as C3′-*endo*, while the value of 89° for dG16 defines this sugar as O1′-*endo* in the adduct duplex. The remaining backbone torsion angles are in or near the range characteristic of a B_I-DNA helical conformation (Table S5).

Convergence to very similar final structures resulted when the lowest energy NMR energy-minimized structure was distorted by +45° or −45° at each of the two bonds (α' and β') at the base–carcinogen linkage and reminimized with restraints. Two views of the best-fit superposition of the resulting four structures are plotted in Figure S3 (Supplementary Material).

DISCUSSION

Spectral Quality. The proton NMR spectra of the (+)-*cis-anti*-[BP]dG·del 11-mer duplex in H_2O buffer at 1 °C (Figure 1A) and in D_2O buffer at 25 °C (Figure 1B) are among the best resolved spectra that we have observed for stereospecific [BP]dG adducts embedded in DNA oligomer duplexes. The NMR studies on the (+)-*cis-anti*-[BP]dG adduct opposite a deletion site could be undertaken at ambient temperature in the present study. By contrast, related NMR studies on the (+)-*cis-anti*-[BP]dG adduct opposite dC had to be undertaken in the 5–10 °C range since we observed the onset of line broadening at ambient temperature (Cosman et al., 1993). Earlier optical melting studies had established that the duplex containing (+)-*cis-anti*-[BP]dG positioned opposite a deletion site was stabilized by 2 °C relative to the same adduct positioned opposite dC (Ya et al., 1994).

We had previously established an equilibrium between a major intercalation–base displacement conformation and a minor groove binding conformation for the (+)-*cis-anti*-[BP]-dG adduct positioned opposite dC based on the observation of exchange cross peaks in NOESY spectra of the (+)-*cis-anti*-[BP]dG·del 11-mer duplex (Cosman et al., 1993). By contrast, no such exchange cross peaks were observed in the present study on the (+)-*cis-anti*-[BP]dG·del 11-mer duplex.

NOE Patterns. The intercalation site alignments and overlap geometries following insertion into the helix of the benzo[a]pyrene ring of the (+)-*cis-anti*-[BP]dG adduct opposite the deletion site and between flanking Watson–Crick dG·dC base pairs (Figure 6) is supported by the experimental NOE patterns observed for the (+)-*cis-anti*-[BP]dG·del 11-mer duplex. Specifically, the alignment of the C^{10}-C^{11}-C^{12} containing long edge of the BP ring toward the d(C5-[BP]-G6-C7) segment of the modified strand (Figure 6B) is supported by the observed NOEs between the BP(H10), BP-(H11), and BP(H12) protons and the sugar protons of dC5, [BP]dG6, and dC7 and the corresponding intermolecular proton–proton separations in the solution structure of the adduct duplex (Tables 2 and S4). This alignment requires the BP(H10) proton to be closer to the dC7 sugar and the BP(H12) proton to be closer to the dC5 sugar (Figure 6B) consistent with the experimental NOEs between these BP protons and the corresponding sugar H1′ protons (Table 2). The alignment of the C^4-C^5-C^6 containing long edge of the BP ring toward the d(G16-G17) segment of the deletion containing strand (Figure 6B) is supported by the observed NOEs between the BP(H3), BP(H4), BP(H5), and BP(H6) protons and the imino and sugar protons of dG16 and dG17 and the corresponding intermolecular proton–proton separations in the solution structure of the adduct duplex (Tables 2 and S4). The C^1-C^2-C^3 edge of the pyrenyl ring of BP is positioned in the major groove, while the C^7-C^8-C^9 edge of the benzylic ring of BP is positioned in the minor groove in the solution structure of the (+)-*cis-anti*-[BP]dG·del 11-mer duplex (Figure 6B). Support for the former observation is based on the observed NOE between the pyrenyl BP(H1) proton and the major groove H5 proton of dC5 which is satisfied by the 3.54-Å distance between these protons in the solution structure (Table 2). Support for the latter observation is based on the observed NOE between the benzylic BP(H10) proton and the minor groove H1′ proton of dC7 which is satisfied by the 4.34-Å distance between these protons in the solution structure (Table 2).

The structural distortion resulting from base displacement of the deoxyguanosine of [BP]dG6 into the minor groove should perturb the NOEs between DNA protons on adjacent residues for the d(C5-[BP]G6-C7)·d(G16-G17) segment centered about the pyrenyl intercalation site in the solution structure of the (+)-*cis-anti*-[BP]dG·del 11-mer duplex. These NOEs are listed as medium, weak, very weak, and absent in Table S6 (Supplementary Material) and are compared with the corresponding intramolecular proton–proton distances in the deduced solution structure. We do not observe sequential NOEs between the H8 proton of [BP]dG6 and the sugar H1′, H2′,2″, and H3′ protons of dC5 for the d(C5-[BP]G6) step consistent with the majority of the distances between these protons being >5.5 Å in the solution structure (Table S6). We observe weak to very weak sequential NOEs between the H6 proton of dC7 and the sugar H1′, H2′,2″, and H3′ protons of [BP]dG6 for the d([BP]G6-C7) step consistent with the majority of the distances between these protons being between 3.5 and 5.0 Å in the solution structure (Table S6). The absence of an NOE between the H8 proton of [BP]dG6 and the H5 proton of dC7 for the purine (3′–5′) pyrimidine d([BP]G6-C7) step is consistent with the orthogonal arrangement of the modified dG6 and dC7 base planes and the 7.89-Å distance between these base protons in the solution structure (Table S6).

The intercalation site generated between the dC5·dG17 and dC7·dG16 base pairs is wedge-shaped, being narrower toward the d(G16-G17) step on the deletion containing strand, in the solution structure of the (+)-*cis-anti*-[BP]dG·del 11-mer duplex (Figure 6A). This is reflected in the 5.76-Å separation between the H8 protons of dG16 and dG17 on the deletion containing strand and the 9.12-Å separation between the H6 protons of dC5 and dC7 on the modification containing strand in the solution structure. We do not observe an NOE between either pair of protons in the adduct duplex consistent with the interproton separations being greater than >5.5 Å for both proton pairs (Table S6). However, the weak NOE between the H8 proton of dG17 and the H1′ proton of dG16 for the d(G16-G17) step is consistent with the 5.08-Å separation between these protons in the solution structure (Table S6).

The modified deoxyguanosine is displaced into the minor groove with its plane positioned over the minor groove face of the sugar ring of dC5 in the structure of the (+)-*cis-anti*-[BP]dG·del 11-mer duplex (Figure 6A). The 4.77-Å separation between the H8 proton of [BP]dG6 and the minor groove H4′ proton of dC5 in the solution structure is consistent with the very weak NOE observed experimentally between these pairs of protons (Table S6).

Chemical Shift Patterns. The intercalated pyrenyl ring stacks primarily over the Watson–Crick edges of the dG16,

dG17, and dC7 bases of the flanking dG·dC base pairs in the solution structure of the (+)-*cis*-*anti*-[BP]dG adduct positioned opposite a deletion site (Figure 6). Consistent with this overlap geometry are the large upfield ring current shifts observed at the imino protons of dG16 (–1.39 ppm) and dG17 (–1.89 ppm) and the amino protons of dC7 (–0.80, –1.12 ppm) and, to a lesser extent, at the amino protons of dC5 (–0.20, –0.82 ppm) on proceeding from the control duplex to the adduct duplex (Table S3). The pyrenyl ring also stacks over the H1′ proton of dC7 in the solution structure of the adduct duplex accounting for the large –1.44 ppm upfield shift for this proton observed experimentally. The H8 and sugar H1′ protons of (+)-*cis*-*anti*-[BP]dG are shifted to low field by +0.24 and +0.59 ppm, respectively (Table S3), consistent with the modified deoxyguanosine being base displaced into the minor groove in the solution structure of the adduct duplex (Figure 6A). The minor groove sugar H1′ and H2″ protons of dC5 are shifted to high field by –0.52 and –1.05 ppm, respectively (Table S3), consistent with the base displaced modified deoxyguanosine ring stacking directly over the minor groove face of dC5 in the solution structure of the adduct duplex (Figure 6A).

The pyrenyl protons are also upfield-shifted in the adduct duplex relative to their unperturbed values in the 8.0–8.5 ppm chemical shift range (Figure 4). This must reflect upfield ring current shifts from the flanking dG·dC base pairs which stack over the intercalated pyrenyl ring system. The BP(H4) proton at 5.72 ppm stacks directly over the purine rings of dG16 and dG17, readily explaining its unusually large upfield shift. The BP(H5) proton at 6.51 ppm and, to a lesser extent, the BP(H3) proton at 6.94 ppm stack over the periphery of the purine rings explaining their upfield shifts relative to other pyrenyl protons (Figure 4).

Comparison of (+)-cis-anti-[BP]dG Adduct Opposite dC and Deletion Site. The solution structure of the central segment of the (+)-*cis*-*anti*-[BP]dG·dC 11-mer duplex (Cosman et al., 1993) and the (+)-*cis*-*anti*-[BP]dG·del 11-mer duplex (this study) are shown in the same relative global orientation of the DNA in Figures 7, panels A and B. Common features include intercalation of the benzo[a]pyrene ring into the helix between intact flanking dG·dC base pairs along with base displacement of the modified deoxyguanosine into the minor groove with its plane parallel to the helix axis and stacked over the minor groove face of the dC5 sugar ring (Figure 7A,B). Both structures exhibit a common distorted half-chair benzylic ring pucker with BP(H7), BP(H8), and BP(H10) in pseudoequatorial orientations while BP(H9) adopts a pseudoaxial orientation.

The carcinogen–base linkage torsion angles α'[dG6(N^1)-dG6(C^2)-dG6(N^2)-BP(C^{10})] are similar for the adduct opposite dC ($\alpha' = 160°$) and opposite a deletion site ($\alpha' = 169°$). By contrast, there is a difference in the carcinogen–base linkage torsion angles β'[dG6(C^2)-dG6(N^2)-BP(C^{10})-BP(C^9)] for the adduct duplex opposite dC ($\beta = 136°$) and opposite a deletion site ($\beta' = 91°$). This difference in β' results in the pyrene ring stacking predominantly over dC5 and dC7 of the modified strand for the adduct positioned opposite dC [Figure 5B of Cosman et al. (1993)] while the pyrene ring is positioned centrally over the base pairing edge but not over the dC5 base for the adduct positioned opposite a deletion site (Figure 6B). This readily explains why the H5 proton of dC5 for the adduct positioned opposite dC (5.17 ppm) (Cosman et al., 1993) resonates to higher field than it does when the adduct is positioned opposite a deletion site (5.56 ppm).

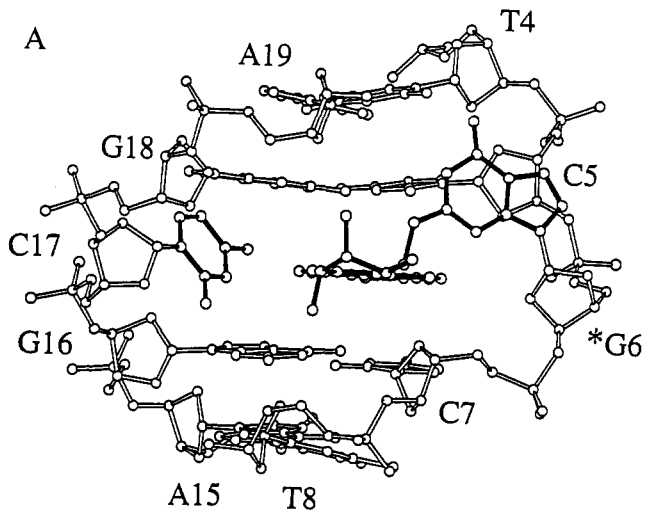

FIGURE 7: Views looking into the minor groove and normal to the helix axis for the solution structures of (A) the d(T4-C5-[BP]G6-C7-T8)·d(A15-G16-C17-G18-A19) segment of the (+)-*cis*-*anti*-[BP]-dG·dC 11-mer duplex and (B) the d(T4-C5-[BP]G6-C7-T8)·d(A15-G16-G17-A18) segment of the (+)-*cis*-*anti*-[BP]dG·del 11-mer duplex. The orientation of the DNA is similar in the two structures.

The unusual sugar pucker and glycosidic torsion angles observed within the d(C5-[BP]G6-C7) segment of the modified strand for the adduct positioned opposite dC (dC5, **P** = 51°; [BP]dG6, χ = 189°) are also observed for the adduct positioned opposite the deletion site (dC5, **P** = 41°; [BP]dG6, χ = 168°).

The flanking dG·dC base pairs are parallel to each other with the deoxycytidine base opposite the adduct looped out of the helix in the (+)-*cis*-*anti*-[BP]dG·dC 11-mer duplex (Figure 7A). By contrast, the intercalation site is wedge-shaped with buckling of the dG bases flanking the deletion site in the (+)-*cis*-*anti*-[BP]dG·del 11-mer duplex (Figure 7B). The flanking dG bases (dG16 and dG18) do not stack on top of each other for the adduct positioned opposite dC (Figure 5B; Cosman et al., 1993) while these dG bases (dG16 and dG17) stack significantly over each other for the adduct positioned opposite the deletion site (Figure 6B). The overlap of the pyrene ring with the deoxyguanosine rings of the flanking dG·dC base pairs is much greater for the adduct positioned

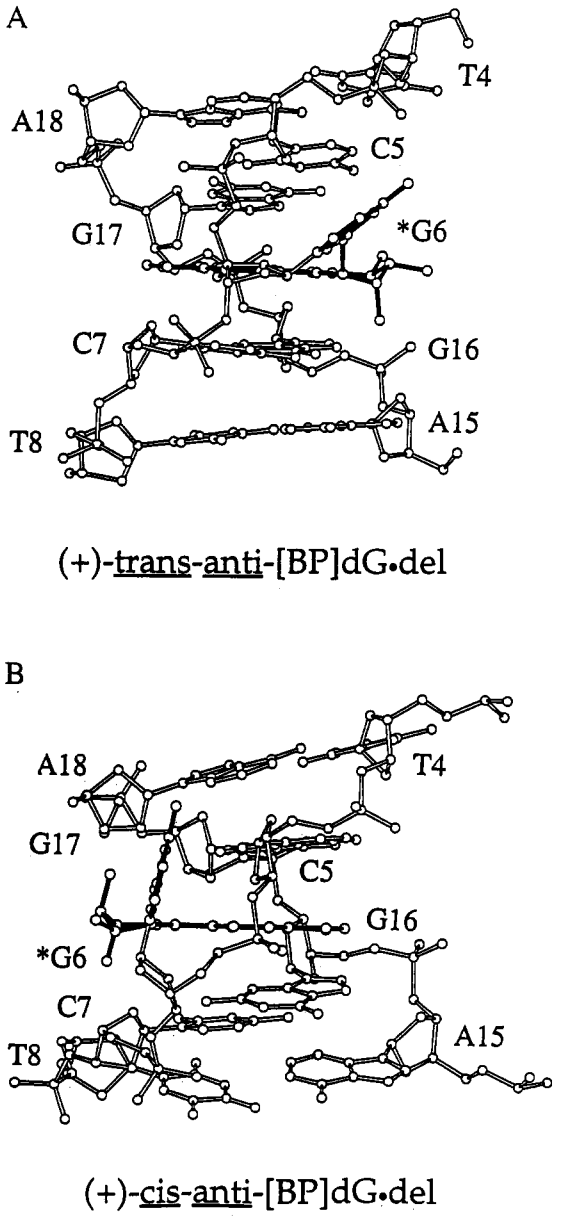

FIGURE 8: Views of the d(T4-C5-[BP]G6-C7-T8)·d(A15-G16-G17-A18) segment of the structures of (A) the (+)-*trans-anti*-[BP]dG·del 11-mer duplex and (B) the (+)-*cis-anti*-[BP]dG·del 11-mer duplex. The orientation of the DNA is similar with the benzo[a]pyrene ring intercalating between flanking dG·dC base pairs in both structures. The deoxyguanosine ring of (+)-*trans-anti*-[BP]dG6 is positioned in the major groove and is tilted relative to the helix axis in panel A while it is positioned in the minor groove and is approximately parallel to the helix axis for the (+)-*cis-anti*-[BP]dG6 stereoisomer in panel B.

opposite the deletion site (Figure 6B) compared to the same adduct positioned opposite dC (Figure 5B; Cosman et al., 1993) accounting for the increased thermal stability of the former [BP]dG·del containing duplex relative to the latter [BP]dG·dC containing duplex (Ya et al., 1994).

Comparison of the (+)-trans-anti- and (+)-cis-anti-[BP]-dG Adducts Opposite Deletion Sites. The solution structures of the d(T4-C5-[BP]G6-C7-T8)·d(A15-G16-G17-G18) segment of the (+)-*trans-anti*-[BP]dG·del 11-mer duplex and the (+)-*cis-anti*-[BP]dG·del 11-mer duplex are shown in Figure 8, panels A and B, respectively. The benzo[a]pyrene ring intercalates between intact Watson–Crick dC5·dG17 and dC7·dG16 base pairs which generate a wedge-shaped intercalation site with base displacement of the deoxyguanosine ring in both structures. The carcinogen–base torsion angles α' are similar for the (+)-*trans-anti*-[BP]dG adduct ($\alpha' = 138°$) and (+)-*cis-anti*-[BP]dG adduct ($\alpha' = 169°$) positioned opposite deletion sites. By contrast, the carcinogen–base linkage torsion angle β' is very different for the (+)-*trans-anti*-adduct ($\beta' = 263°$) and (+)-*cis-anti*-adduct ($\beta' = 91°$) indicative of an approximately 180° flip at this linkage angle between the two stereoisomers.

Strikingly, the benzylic ring of the benzo[a]pyrene and the attached base displaced deoxyguanosine are positioned in the major groove for the (+)-*trans-anti*-adduct stereoisomer (Figure 8A) and the minor groove for the (+)-*cis-anti*-adduct stereoisomer (Figure 8B) positioned opposite deletion sites. The purine base of [BP]dG6 is aligned at an angle of 140° for the (+)-*trans-anti*-adduct stereoisomer (Figure 8A) and at an angle of 80° for the (+)-*cis-anti*-adduct stereoisomer (Figure 8B) relative to the intercalated benzo[a]pyrene ring. Further, different values are observed for the [BP]dG6 glycosidic torsion angle in the (+)-*trans-anti*-adduct ($\chi = 301°$) and the (+)-*cis-anti*-adduct ($\chi = 168°$) positioned opposite deletion sites. The modified deoxyguanosine stacks over the major groove base protons (H5 and H6) of dC5 in the (+)-*trans-anti*-adduct stereoisomer (Figure 8A) and stacks over the minor groove face sugar protons (H1′, H2″ and H4′) of dC5 in the (+)-*cis-anti*-adduct stereoisomer (Figure 8B). The majority of the sugar puckers are C2′-*endo* in both structures except that dC7 is C3′-*endo* in the (+)-*trans-anti*-[BP]dG·del structure while dC5 is C3′-*endo* in the (+)-*cis-anti*-[BP]dG·del structure.

General Conclusions. Our previous structural research established that the (+)-*trans-anti*- and (+)-*cis-anti*-[BP]-dG stereoisomers adopted totally different conformations when positioned opposite dC in a DNA duplex. The benzo[a]pyrene ring is positioned in the minor groove without disruption of the [BP]dG·dC base pair in the former structure (Cosman et al., 1992); while the modified base pair was disrupted in the latter structure with the [BP]dG displaced into the minor groove, the dC positioned opposite it displaced into the major groove, and the benzo[a]pyrene intercalating into the resulting cavity within the helix (Cosman et al., 1993).

By contrast, independent of the stereoisomer under consideration, the benzo[a]pyrene ring intercalates into the helix when either the (+)-*trans-anti*- or the (+)-*cis-anti*-[BP]dG adduct is positioned opposite a deletion site. Thus, it appears that the pyrenyl ring which is larger than the deoxyguanosine ring preferably intercalates between flanking intact dG•dC base pairs for benzo[a]pyrene adduct linked to the N^2 position of the dG residue and positioned opposite a deletion site. The different stereoisomers of [BP]dG position the base-displaced modified deoxyguanosine in different grooves so that one can anticipate differential recognition and repair of individual stereoisomeric [BP]dG lesions positioned opposite deletion sites at the duplex level.

This study with a (+)-*cis-anti*-[BP]dG lesion and the previous one with a (+)-*trans-anti*-[BP]dG lesion suggest that the hydrophobic pyrenyl residues, when positioned opposite deletion sites, are localized at intercalation-like sites in which contact with the aqueous solvent environment is minimized. Similar preferences for intercalation at bulged binding sites have been observed in the case of other polynuclear aromatic ligands which bind noncovalently to DNA. Bulky ligands such as acridine orange, ethidium bromide, and other intercalators have a greater affinity for binding to bulged bases in DNA (Turner, 1992; Nelson & Tinoco, 1985; Woodson & Crothers, 1988: Williams & Goldberg, 1988) and RNA (White & Draper, 1989) than to normal duplex

regions. Our findings with the covalently linked [BP]dG lesion positioned opposite single-base deletion sites in oligonucleotide duplexes suggest some plausible reasons for complex formation at bulged sites. In normal duplexes with the dC present on the partner strand opposite the lesion, the bulky BP residue in (+)-*trans*-*anti*-[BP]dG lesions prefers a minor groove conformation (Cosman et al., 1992). The fact that an intercalative conformation is preferred for (+)-*trans*-*anti*-[BP]dG and (+)-*cis*-*anti*-[BP]dG lesions when the dC is deleted suggests that ligand–base pair stacking interactions are important in determining the structures of these complexes. An additional favorable factor is that the bulky BP residue can fit into the bulged sites without disrupting the hydrogen bonding of adjacent base pairs.

Finally, our results demonstrate that stable duplexes with (+)-*anti*-[BP]dG lesions positioned opposite deletion sites in DNA oligonucleotides can be formed. Structural intermediates of this type may account for the sizeable fractions of deletion mutations found in primer extension experiments catalyzed by the Klenow fragment of DNA polymerase Pol 1 (without the exonuclease proofreading activity) *in vitro* (Shibutani et al., 1993).

Future Studies. The structural characterization of the stereochemically distinct [BP]dG adducts positioned opposite −1 deletion sites reported in these two papers can be extended to higher resolution by refining the structures directly against the NOE intensities. These studies will be undertaken once we complete our current efforts to develop efficient refinement protocols for the high-resolution structural characterization of covalent carcinogen–DNA adducts.

We shall next attempt to structurally characterize stereochemically distinct [BP]dG adducts positioned opposite −2 deletion sites since such frame-shift mutations have been detected in *in vitro* DNA polymerase catalyzed primer extension experiments (Shibutani et al., 1993). It is not possible to *a priori* predict whether the pyrenyl ring of [BP]-dG adducts will intercalate into the helix opposite −2 deletion sites and, if so, what conformation(s) will be adopted by the two residue bulge which contains the lesion site.

SUPPLEMENTARY MATERIAL AVAILABLE

Six tables listing exchangeable proton and nonexchangeable proton chemical shifts as well as proton chemical shift differences on adduct formation, backbone torsion angles of the lowest energy structure for the central trinucleotide segment, and a comparison of intermolecular and intramolecular nucleic acid proton–proton separations with the corresponding magnitude of experimental NOEs for the adduct duplex and four figures showing an expanded NOESY contour plot in D_2O, phosphorus chemical shifts on adduct formation, two views of the entire the adduct duplex, and the superposition of four structures derived following energy minimization with constrains from the lowest energy structure of the adduct duplex in which the α' and β' angles were changed by ±45° (13 pages). Ordering information is given on any current masthead page.

REFERENCES

Bernelot-Moens, C., Glickman, B. W., & Gordon, A. J. E. (1990) *Carcinogenesis 11*, 781–785.

Carothers, A. M., & Grunberger, D. (1990) *Carcinogenesis 11*, 189–192.

Cheng, S. C., Hilton, B. D., Roman, J. M., & Dipple, A. (1989) *Chem. Res. Toxicol. 2*, 334–340.

Conney, A. H. (1982) *Cancer Res. 42*, 4875–4917.

Cosman, M. (1991) Ph.D. Dissertation, New York University, New York.

Cosman, M., de los Santos, C., Fiala, R., Hingerty, B. E., Singh, S. B., Ibanez, V., Margulis, L. A., Live, D., Geacintov, N. E., Broyde, S., & Patel, D. J. (1992) *Proc. Natl. Acad. Sci. U.S.A. 89*, 1914–1918.

Cosman, M., de los Santos, C., Fiala, R., Hingerty, B. E., Luna, E., Harvey, R. G., Geacintov, N. E., Broyde, S., & Patel, D. J. (1993) *Biochemistry 32*, 4145–4155.

Cosman, M., Fiala, R., Hingerty, B. E., Amin, S., Geacintov, N. E., Broyde, S., & Patel, D. J. (1994) *Biochemistry* (preceding paper in this issue).

Harvey, R. G. (1991) *Polycyclic Aromatic Hydrocarbons: Chemistry and Carcinogenicity*, Cambridge University Press.

Jeffrey, A. M., Jennette, K. W., Blobstein, S. H., Weinstein, I. B., Beland, F. A., Harvey, R. G., Kasai, H., Miura, I., & Nakanishi, K. (1976) *J. Am. Chem. Soc. 98*, 5714–5715.

Keohavong, P., & Thilly, W. G. (1992) *Proc. Natl. Acad. Sci. U.S.A.* 89, 4623–4627.

Koreeda, M., Moore, P. D., Wislocki, P. G., Levin, W., Conney, A. H., Yagi, H., & Jerina, D. M. (1978) *Science 199*, 778–781.

Kunkel, T. A. (1990) *Biochemistry 29*, 8003–8011.

Lambert, I. B., Napolitano, R. L., & Fuchs, R. P. (1992) *Proc. Natl. Acad. Sci. U.S.A. 89*, 1310–1314.

Mackay, W., Benasutti, M., Drouin, E., & Loechler, E. L. (1992) *Carcinogenesis 13*, 1415–1425.

Maher, V. M., Yang, J.-L., Ma, M. C.-M., & McCormick, J. (1989) *Mutation Res. 220*, 83–92.

Mazur, M., & Glickman, B. W. (1988) *Somat. Cell. Mol. Genet. 14*, 393–400.

Mizusawa, H., Lee, C.-H., Kakefuda, T., McKenney, K., Shimatake, H., & Rosenberg, M. (1981) *Proc. Natl. Acad. Sci. U.S.A. 78*, 6817–6820.

Nelson, J. W., & Tinoco, I., Jr. (1985) *Biochemistry 24*, 6416–6421.

Rodriguez, H., & Loechler, E. L. (1993) *Carcinogenesis 14*, 373–383.

Schaaper, R. M., Koffel-Schwarz, N., & Fuchs, R. P. (1990) *Carcinogenesis 11*, 1087–1095.

Shibutani, S., & Grollman, A. P. (1993) *J. Biol. Chem. 268*, 11703–11710.

Shibutani, S., Margulis, L. A., Geacintov, N. E., & Grollman, A. P. (1993) *Biochemistry 32*, 7531–7541.

Stevens, C. W., Bouck, N., Burgess, J. A., & Fahl, W. E. (1985) *Mutat. Res. 152*, 5–14.

Streisinger, G., Okada, Y., Emrich, J., Newton, J., Tsugita, A., Terzaghi, F., & Inouye, M. (1966) *Cold Spring Harbor Symp. Quant. Biol. 31*, 77–84.

Turner, D. H. (1992) *Curr. Opin. Struct. Biol. 2*, 334–337.

Wei, S. J. C., Chang, R. L., Wong, C.-Q., Bhachech, N., Cui, X. X., Hennig, E. Yagi, H., Sayer, J. M., Jerina, D. M., Preston, B. D., & Conney, A. H. (1991) *Proc. Natl. Acad. Sci. U.S.A. 88*, 11227–11230.

Wei, S. J. C., Chang, R. L., Bachech, N., Cui, X. X., Merkler, K. A., Wong, C. Q., Hennig, E., Yagi, H., Jerina, D. M., & Conney, A. H. (1993) *Cancer Res. 53*, 3294–3301.

Woodson, S. A., & Crothers, D. M. (1988) *Biochemistry 27*, 8904–8914.

Williams, L. D., & Goldberg, I. H. (1988) *Biochemistry 27*, 3004–3011.

White, S. A., & Draper, D. E. (1989) *Biochemistry 28*, 1892–1897.

Ya, N.-Q., Smirnov, S., Cosman, M., Bhanot, S., Ibanez, V., & Geacintov, N. E. (1994) *Proceedings: 8th Conversation Biomolecular Stereodynamics* (Sarma, R. H., & Sarma, M. H., Eds.) pp 349–366, Adenine Press, Schenectady, New York.

Yang, J.-L., Maher, V. M., & McCormick, J. (1987) *Proc. Natl. Acad. Sci. U.S.A. 84*, 3787–3791.

Yang, J.-L., Chen, R.-H., Maher, V. M., & McCormick, J. (1991) *Carcinogenesis 12*, 71–75.